

RESEARCH

Open Access



# miR-128-3p inhibits intramuscular adipocytes differentiation in chickens by downregulating *FDPS*

Shuaipeng Zhu<sup>1†</sup>, Binbin Zhang<sup>1†</sup>, Tingqi Zhu<sup>1</sup>, Dongxue Wang<sup>1</sup>, Cong Liu<sup>1</sup>, Yixuan Liu<sup>1</sup>, Yuehua He<sup>1</sup>, Wenjie Liang<sup>1</sup>, Wenting Li<sup>1,2</sup>, Ruili Han<sup>1,2</sup>, Donghua Li<sup>1</sup>, Fengbin Yan<sup>1</sup>, Yadong Tian<sup>1</sup>, Guoxi Li<sup>1,2</sup>, Xiangtao Kang<sup>1,2</sup>, Zhuanjian Li<sup>1</sup>, Ruirui Jiang<sup>1</sup> and Guirong Sun<sup>1,2\*</sup>

## Abstract

**Background** Intramuscular fat (IMF) content is the major indicator for evaluating chicken meat quality due to its positive correlation with tenderness, juiciness, and flavor. An increasing number of studies are focusing on the functions of microRNAs (miRNAs) in intramuscular adipocyte differentiation. However, little is known about the association of miR-128-3p with intramuscular adipocyte differentiation. Our previous RNA-seq results indicated that miR-128-3p was differentially expressed at different periods in chicken intramuscular adipocytes, revealing a possible association with intramuscular adipogenesis. The purpose of this research was to investigate the biological functions and regulatory mechanism of miR-128-3p in chicken intramuscular adipogenesis.

**Results** The results of a series of assays confirmed that miR-128-3p could promote the proliferation and inhibit the differentiation of intramuscular adipocytes. A total of 223 and 1,050 differentially expressed genes (DEGs) were identified in the mimic treatment group and inhibitor treatment group, respectively, compared with the control group. Functional enrichment analysis revealed that the DEGs were involved in lipid metabolism-related pathways, such as the MAPK and TGF- $\beta$  signaling pathways. Furthermore, target gene prediction analysis showed that miR-128-3p can target many of the DEGs, such as *FDPS*, *GGT5*, *TMEM37*, and *ASL2*. The luciferase assay results showed that miR-128-3p targeted the 3' UTR of *FDPS*. The results of subsequent functional assays demonstrated that miR-128-3p acted as an inhibitor of intramuscular adipocyte differentiation by targeting *FDPS*.

**Conclusion** miR-128-3p inhibits chicken intramuscular adipocyte differentiation by downregulating *FDPS*. Our findings provide a theoretical basis for the study of lipid metabolism and reveal a potential target for molecular breeding to improve meat quality.

**Keywords** Chicken, Intramuscular adipocyte, RNA-seq, MiR-128-3p, *FDPS*, Adipogenesis

## Background

Poultry meat is an important animal origin food source which can provide essential nutrients [1]. The nutritional value of poultry meat has recently received tremendous attention [2]. A Chinese local chicken breed, Gushi chicken is favored by most consumers for its delicious and uniquely flavored meat. Intramuscular fat (IMF) content is an important indicator affecting

<sup>†</sup>Shuaipeng Zhu and Binbin Zhang are co-first authors.

\*Correspondence:

Guirong Sun  
grsun2000@126.com

<sup>1</sup> College of Animal Science and Technology, Henan Agricultural University, Zhengzhou 450046, P.R. China

<sup>2</sup> The Shennong Seed Industry Laboratory, Zhengzhou 450002, China



many aspects of poultry meat quality, including flavor, tenderness, and taste [3, 4]. IMF deposition depends mainly on hypertrophy and hyperplasia of adipocytes [5–7]. IMF deposition studies have been reported in major livestock and poultry species, such as cattle [8], sheep [9], and chickens [10]. Our previous studies showed significant differences in the density and size of lipid droplets in breast muscle between the early and late stages of egg laying as well as between groups [11]. Therefore, an in-depth study of adipocyte proliferation and differentiation is particularly important.

MicroRNAs (miRNAs) are short noncoding RNAs of approximately 22 nucleotides that negatively regulate gene expression at the posttranscriptional level by recognizing the 3' UTR of a target mRNA [12–14]. Studies have shown that miRNAs are involved in regulating various biological processes, including lipid metabolism, adipogenesis, cell proliferation and cell differentiation [15–17]. For instance, miR-33a inhibits the differentiation of bovine preadipocytes through the IRS2-Akt pathway [18]. The miR-429-3p/LPIN1 axis promotes chicken abdominal fat deposition via the *PPAR $\gamma$*  pathway [19], while miR-130a suppresses adipogenic differentiation of BMSCs by targeting *PPAR $\gamma$*  [20]. Recent studies have also suggested that miR-128-3p may be involved in the regulation of fat deposition in humans [21], mice [22] and chickens [23]. For example, miR-128-3p may target *IRS-1*, *FOXO1*, *SREBP-1c/2* and *ChREBP*, which are functionally involved in lipid and lipoprotein metabolism as well as insulin signaling [24]. In addition, miR-128-3p has a targeting relationship with the adipose differentiation marker gene *PPAR $\gamma$*  [23]. Moreover, our previous transcriptome analysis found significant differences in the expression of miR-128-3p before and after intramuscular adipocyte differentiation, and we thus speculated that miR-128-3p may be a core miRNA regulating intramuscular adipose differentiation [25]. However, the regulatory mechanism of miR-128-3p in chicken intramuscular adipogenesis remains unclear.

In this study, we verified the effect of miR-128-3p in intramuscular adipocytes of Gushi chickens and compared the dynamic changes in lipid metabolism after miR-128-3p overexpression and interference. We identified several key mRNAs that play a role in the regulation of lipid metabolism pathways via miR-128-3p using transcriptome data and functional prediction. In addition, the results of our cell functional assays confirmed that miR-128-3p regulates the differentiation of intramuscular adipocytes in chickens. Our findings also provide valuable prospects for clarifying the process of IMF deposition in chickens and further contribute to the improvement of meat quality in farm animals.

## Results

### miR-128-3p promotes the proliferation of chicken intramuscular adipocytes

Intramuscular adipocytes were transfected with the miR-128-3p mimic or inhibitor or with the negative control (NC) for 24 h. RT-qPCR analysis showed that the miR-128-3p expression level was significantly increased in intramuscular adipocytes transfected with the miR-128-3p mimic compared to the NC ( $P < 0.001$ ) (Fig. S1A) and was significantly decreased by transfection of the miR-128-3p inhibitor compared to the NC ( $P < 0.001$ ) (Fig. S1B). These results indicated that the transfection experiment was effective and guaranteed the reliability of the data obtained in follow-up investigations. In chicken intramuscular adipocytes, overexpression of miR-128-3p significantly increased the expression of the marker genes *BCL2* and *PCNA*, which promote cell proliferation, and significantly decreased the expression of *P21*, which inhibits cell proliferation ( $P < 0.05$ ) (Fig. 1A). In contrast, miR-128-3p inhibition significantly decreased the expression of *BCL2* and *PCNA* and significantly increased the expression of *P21* ( $P < 0.05$ ) (Fig. 1B). The results of the CCK-8 assay showed that overexpression of miR-128-3p promoted the proliferation of intramuscular adipocytes, whereas inhibition of miR-128-3p inhibited the proliferation of intramuscular adipocytes (Fig. 1C). The results of the EdU incorporation assay showed that the proportion of EdU-positive cells increased and decreased correspondingly after miR-128-3p overexpression and interference, respectively (Fig. 1D, E). To further confirm the role of miR-128-3p in the proliferation of chicken intramuscular adipocytes, we conducted overexpression experiments. Upon miR-128-3p overexpression, the numbers of cells in S phase and G2 phase increased significantly ( $P < 0.05$ ), while the number of cells in G1 phase decreased (Fig. 1F, Fig. S2). The results of the apoptosis assay showed that the apoptosis rate decreased dramatically after transfection with the miR-128-3p mimic ( $P < 0.05$ ) (Fig. 1G, Fig. S3). The opposite effects were observed when the expression of miR-128-3p was down-regulated ( $P < 0.05$ ). All above indicate that miR-128-3p may promote the proliferation of chicken intramuscular adipocytes.

### miR-128-3p inhibits the differentiation of chicken intramuscular adipocytes

The expression of adipogenic genes (*FABP4*, *FASN*, and *CEBPA*) was measured in chicken intramuscular adipocytes following transfection. The expression of the adipocyte differentiation marker genes *FABP4* and *CEBPA*, which promote fat deposition, was substantially decreased and increased after miR-128-3p overexpression and interference, respectively ( $P < 0.05$ ) (Fig. 2A,

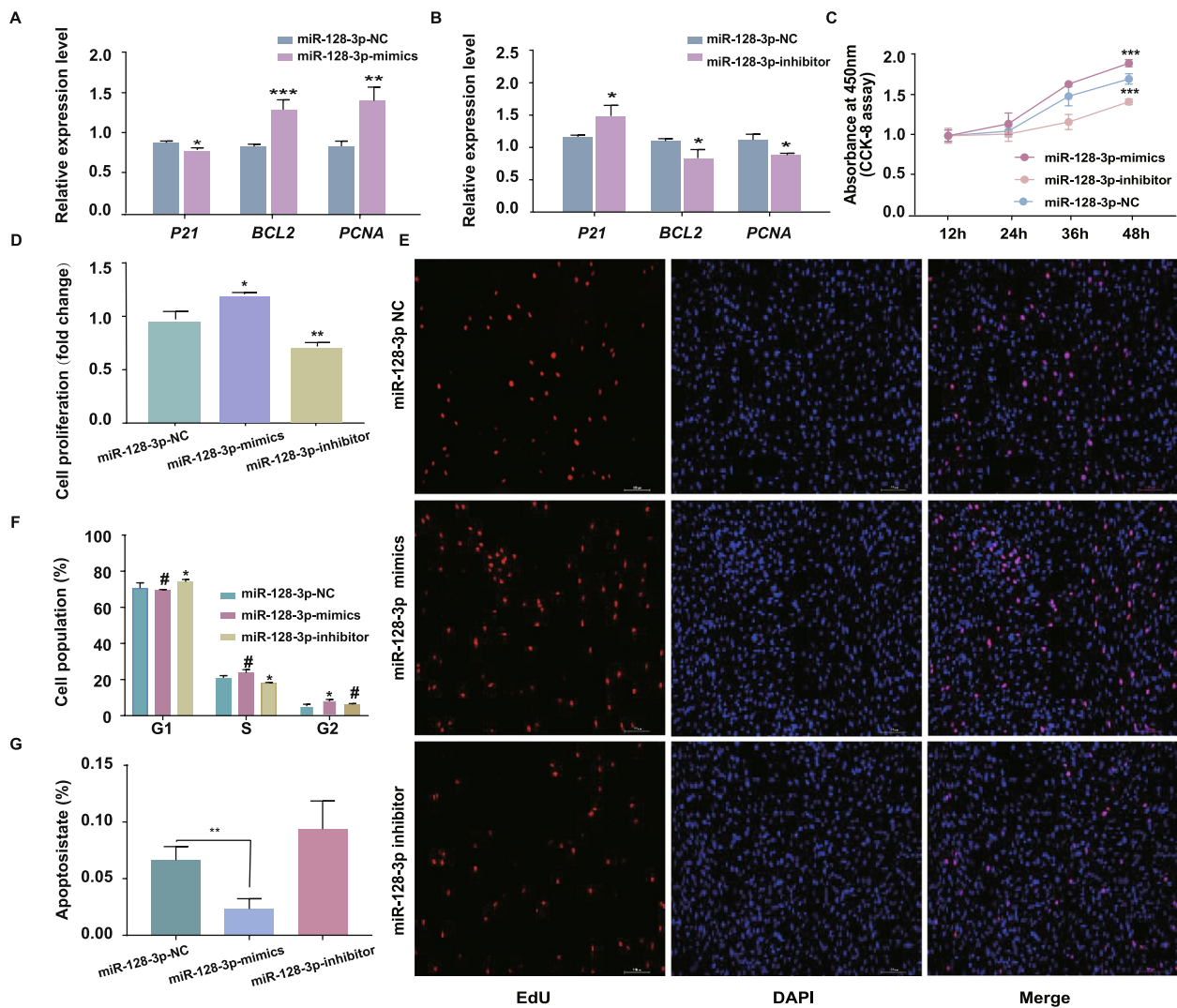


**Fig. 1** miR-128-3p promoted the proliferation of intramuscular adipocytes. **A, B** Relative mRNA levels of cell proliferation-related genes (*P21*, *BCL2*, *PCNA*) after miR-128-3p overexpression or interference. **C** Cell growth curves determined by a CCK-8 assay at 12 h, 24 h, 36 h, and 48 h following miR-128-3p overexpression or interference. **D** Proliferation state of preadipocytes, as assessed by an EdU incorporation assay, after miR-128-3p overexpression or interference. **E** Cell cycle analysis via flow cytometry after miR-128-3p overexpression or interference. **F** Apoptosis assay via flow cytometry after miR-128-3p overexpression or interference. The results are shown as the mean ± S.E.M. values, and the data are representative of at least three independent assays. Independent samples t tests were used to analyze the significance of differences between groups (#  $P > 0.05$ , \*  $P < 0.05$ ; \*\*  $P < 0.01$ , \*\*\*  $P < 0.001$ )

B). We next sought to further investigate the effect of adipocyte differentiation on lipid droplet accumulation and intracellular triglyceride (TG) content in chickens. Oil Red O staining demonstrated that overexpression of miR-128-3p greatly decreased lipid accumulation in intramuscular adipocytes ( $P < 0.05$ ) (Fig. 2C, D) and that miR-128-3p inhibitor transfection had the opposite effect on adipogenesis ( $P < 0.05$ ) (Fig. 2C, E). In addition, the results of the triglyceride assay showed that overexpression of miR-128-3p decreased intracellular triglycerides ( $P < 0.01$ ) (Fig. 2F) but interference with miR-128-3p

increased intracellular triglycerides (Fig. 2G). Summarize the above, these data that indicate miR-128-3p has the ability to prevent chicken intramuscular adipocytes from differentiating.

### Transcriptome data analysis and screening of miR-128-3p target genes

To further explore the gene regulatory pattern associated with miR-128-3p in intramuscular adipocytes and screen for downstream regulated genes, we performed transcriptome sequencing of intramuscular adipocytes



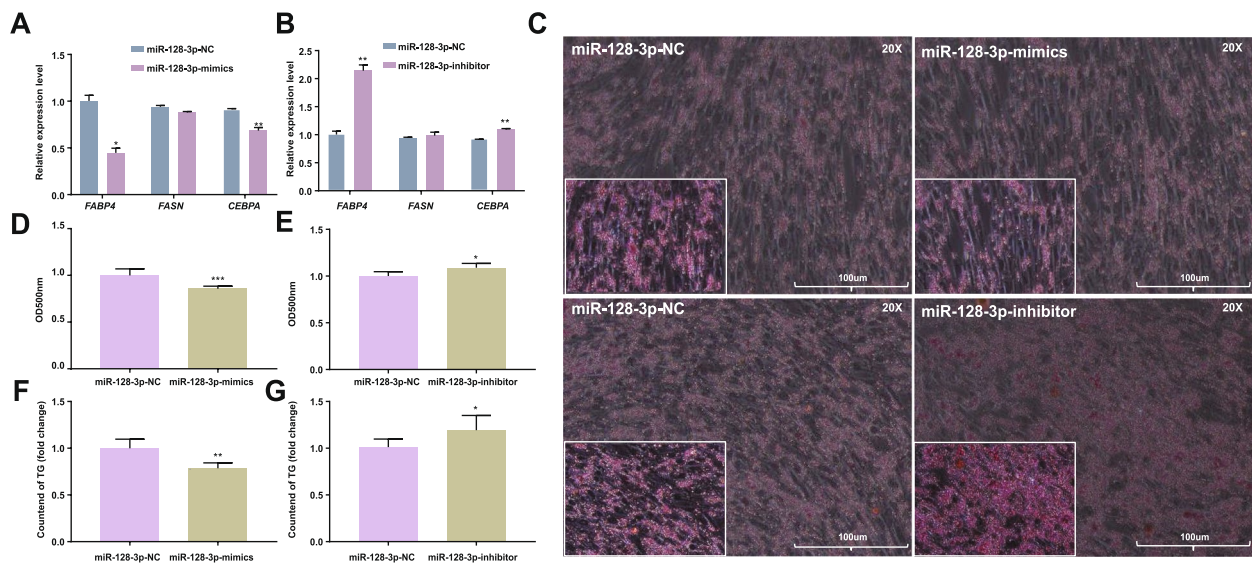


**Fig. 2** miR-128-3p inhibited the differentiation of chicken intramuscular adipocytes. **A, B** Relative mRNA levels of cell proliferation-related genes (*FABP4*, *FASN* and *CEBPA*) after miR-128-3p overexpression or interference. **C** Representative images of Oil Red O staining in intramuscular adipocytes transfected with the miR-128-3p mimic, miR-128-3p inhibitor or corresponding NC (this image was acquired with a 20× objective, and an enlarged image is shown in the bottom left corner of the image). **D, E** Semiquantitative assessment of Oil Red O absorbance at 450 nm. **F, G** The triglyceride content was determined by measurement of the absorbance at 500 nm after miR-128-3p overexpression or interference

after transfection with the miR-128-3p mimic and inhibitor. The clean reads were compared with the reference genome (*Gallus\_gallus-7.0*), and the results showed that the average mapping rate of the clean reads was higher than 97% (Supplementary Table 2–4). The distribution of reads aligning to the genome was determined, and the findings indicated that approximately 85% of the reads were distributed on genes, approximately 15% of the reads were distributed in intergenic regions, and more than 90% of the reads were distributed in exonic regions (Supplementary Table 5). To explore the mRNA changes and biological clustering across groups, we first performed principal component analysis (PCA). PCA for the three groups showed that 92% of the variance could be explained by the first two principal components (Fig. 3A), indicating the diverse mRNA profiles across these three groups. To confirm the reliability of the RNA-seq results, six DEGs (*CNCNB3*, *CHRD2*, *FDPS*, *FMO3*, *PDGFRA*, and *STK32C*) were randomly selected, and their expression levels were measured by RT-qPCR (Fig. 3B). As expected, the expression levels of all six candidate genes showed a consistent trend of expression, therefore validating our results.

A total of 1,689 differentially expressed mRNAs, namely, 817 upregulated and 862 downregulated mRNAs, were identified by comparing the overexpression group (M group) with the interference group (SI group) (Fig. 3C). Functional enrichment analysis revealed that the DEGs were involved in lipid metabolism-related

pathways, such as the MAPK and TGF- $\beta$  signaling pathways (Fig. S4C, F). These DEGs, such as *APOA1*, *FDPS*, *MSMO1*, and *HMGCS1*, were identified to potentially regulate chicken preadipocyte differentiation (Supplementary Table 6). Upregulated miRNAs affect fat accumulation by downregulating their target mRNAs. Therefore, we performed network interaction analysis using Cytoscape software and plotted the regulatory network of miR-128-3p. In this network, miR-128-3p can target 56 down regulated DEGs, such as *FDPS*, *GGT5*, *TMEM37*, and *ASL2*, based on the comparison of binding sites in the miR-128-3p seed region (Fig. 3D). Enrichment analysis showed that these potential target genes were mainly involved in metabolic pathways, including steroid biosynthesis and terpenoid backbone and butanoate metabolism (Fig. 3E). To ensure that the selected target genes indeed play a role in IMF deposition, we investigated whether these potential target genes overlapped among the three comparisons (NC vs. M, NC vs. SI, and SI vs. M). The intersection of the overlapping genes indicated that 34 DEGs were potential target genes of miR-128-3p (Fig. 3F, Table S7).

#### FDPS as a target gene of miR-128-3p

We predicted the binding capacity of the gene 3'UTR region of miR-128-3p using an online website (<https://bibiserv.cebitec.unibielefeld.de/rnahybrid/submission.html/>). The results showed that *FDPS* had strong binding ability with both miR-128-3p (Fig. 4A, B). To validate

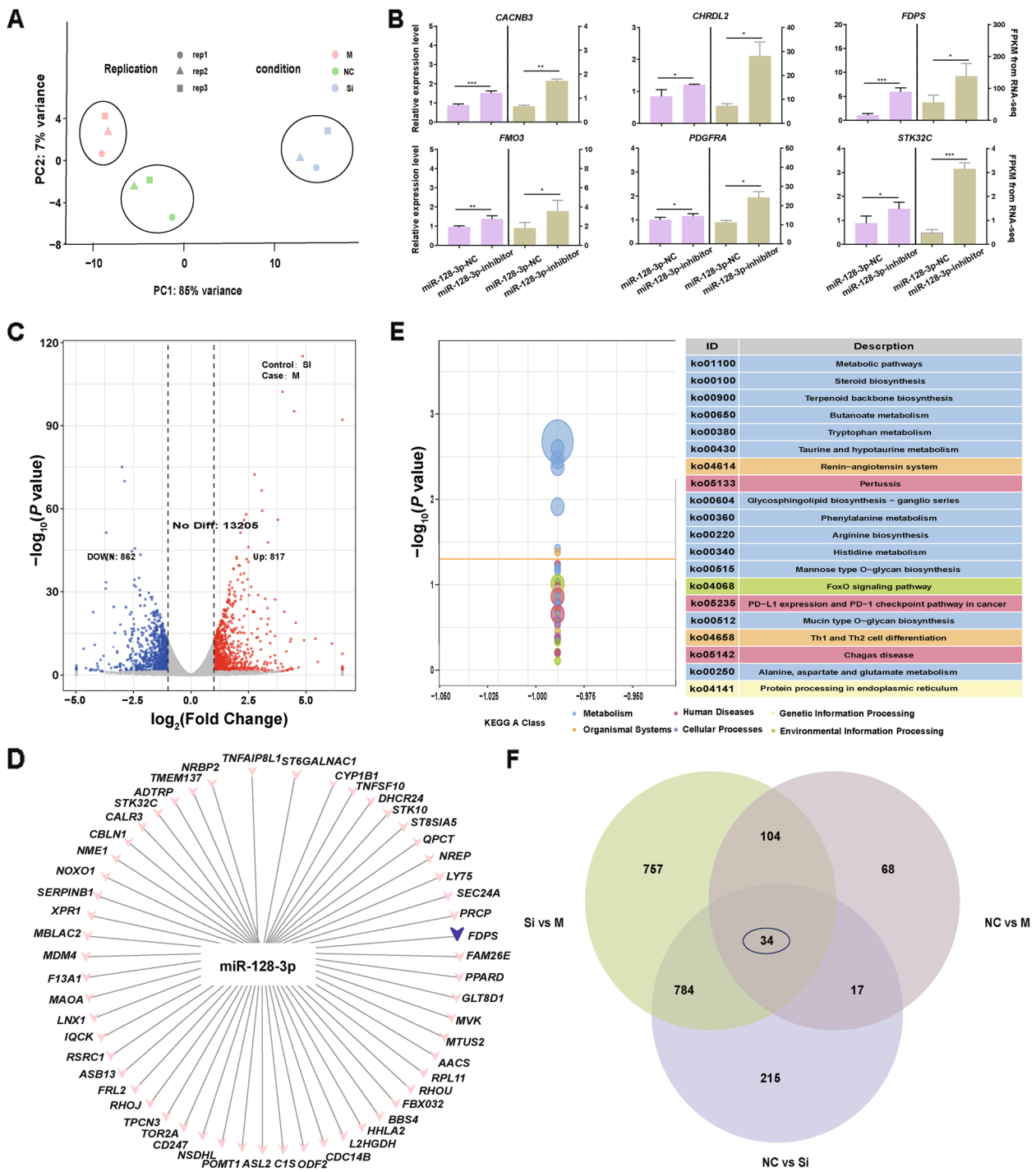


**Fig. 3** Differential mRNA expression analysis. **A** PCA of the samples. **B** Validation of mRNA sequencing data. **C** Volcano plot of gene expression in the SI vs. M comparison. Numbers of upregulated and downregulated differentially expressed mRNAs. The left blue bars represent the numbers of upregulated genes; the orange bars represent the numbers of downregulated genes. **D** Based on the comparison of binding sites in the seed region of miR-128-3p, Cytoscape software was used for network interaction analysis, and the regulatory network of miR-128-3p was mapped. **E** KEGG pathway enrichment analysis of the DEGs in the M vs. SI comparison. **F** Venn diagrams of DEGs identified by RNA-seq in the NC vs. M, NC vs. SI, and SI vs. M comparisons

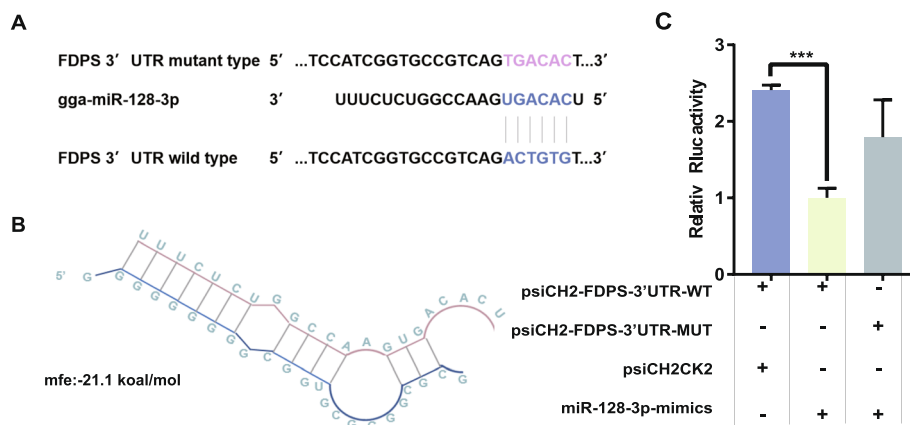


**Fig. 4** *FDPS* as a target gene of miR-128-3p. **A** The potential miR-128-3p target site in the *FDPS* mRNA 3'UTR was predicted by the RNAhybrid tool. **B** The miR-128-3p binding site in the *FDPS* mRNA 3'UTR. **C** A dual luciferase reporter assay was performed by cotransfecting plasmids containing the wild-type or mutated *FDPS* 3'UTR, the psiCH2CK2 plasmid and the miR-128-3p mimic into DF-1 cells. The results are shown as the mean  $\pm$  S.E.M. values, and the data are representative of at least three independent assays. Independent samples t tests were used to analyze the significance of differences between groups (\*\*\*)  $P < 0.001$

this prediction, we then performed dual luciferase report assay, and the results supported that miR-128-3p mimics can significantly inhibit the luciferase activity of psiCHECK2-*FDPS* 3'UTR-WT. However, it has no effect on psiCHECK2-*FDPS* 3'UTR-MuT (Fig. 4C). It indicated that *FDPS* gene and miR-128-3p were in a targeted binding relationship.

#### Interference with *FDPS* inhibits intramuscular preadipocytes differentiation

To verify whether *FDPS* and miR-128-3p exert opposing regulatory effects on fat deposition, we conducted in vitro experiments to investigate the effect of *FDPS* on intramuscular adipocyte differentiation. During intramuscular preadipocyte differentiation, an increasing trend was observed in the expression of *FDPS* from 0 to 10 d, suggesting that *FDPS* may be related to adipose differentiation as a target gene (Fig. 5A). To further investigate the effect of *FDPS* interference on lipid deposition in intramuscular adipocytes, *FDPS* small interfering RNAs (siRNAs) were transfected into intramuscular adipocytes. Compared with that in the NC cells, the expression level of *FDPS* in transfected intramuscular adipocytes was decreased (Fig. 5B). Quantitative real-time PCR analysis showed that the expression of adipose differentiation marker genes (*CEBPA* and *PPARG*) was significantly reduced ( $P < 0.01$ ), but there was no significant change in the expression level of *FABP4* (Fig. 5C). The results of the triglyceride assay indicated that interfering with *FDPS* gene expression reduced the triglyceride content (Fig. 5D). Moreover, Oil Red O staining showed that interfering with *FDPS* gene expression reduced lipid accumulation (Fig. 5E, F) ( $P < 0.001$ ). Therefore, these

findings further confirm that miR-128-3p can inhibit intramuscular adipocyte differentiation by regulating the expression of *FDPS*.

#### Discussion

Compared with nutritional regulation and feeding management on IMF content, regulation of genetic factors has a more precise influence on IMF accumulation in skeletal muscle [26]. miRNAs can normally bind to the 3'UTRs of their target mRNAs and function as endogenous translational repressors [27]. Thus, miRNAs also play a key role in meat quality and growth performance in livestock and poultry [28, 29]. For example, gga-miRNA-18b-3p can inhibit the differentiation of chicken intramuscular adipocytes by targeting *ACOT13* [25], and miR-223 can inhibit intramuscular adipocyte differentiation by targeting *GPAM* [30]. Our results showed that miR-128-3p promoted intramuscular preadipocyte proliferation to some extent. However, a pair of studies showed that miR-128-3p inhibits hepatocellular carcinoma (HCC) cell proliferation by binding to *PIK3R1* [31] and *CDC6* [32]. Moreover, via repression of *FOXO4* and *MMP9* gene expression, the proliferation of vascular smooth muscle cells was inhibited [33]. These observations reveal that miR-128-3p may play different roles in different cell types. Furthermore, we experimentally determined that miR-128-3p inhibited chicken intramuscular adipocyte differentiation, consistent with the findings of other studies [22, 34, 35].

Identifying the miRNA-mRNA regulatory network is important for in-depth study of the mechanisms regulating intramuscular adipocyte development. Above, we showed that miR-128-3p was involved in intramuscular

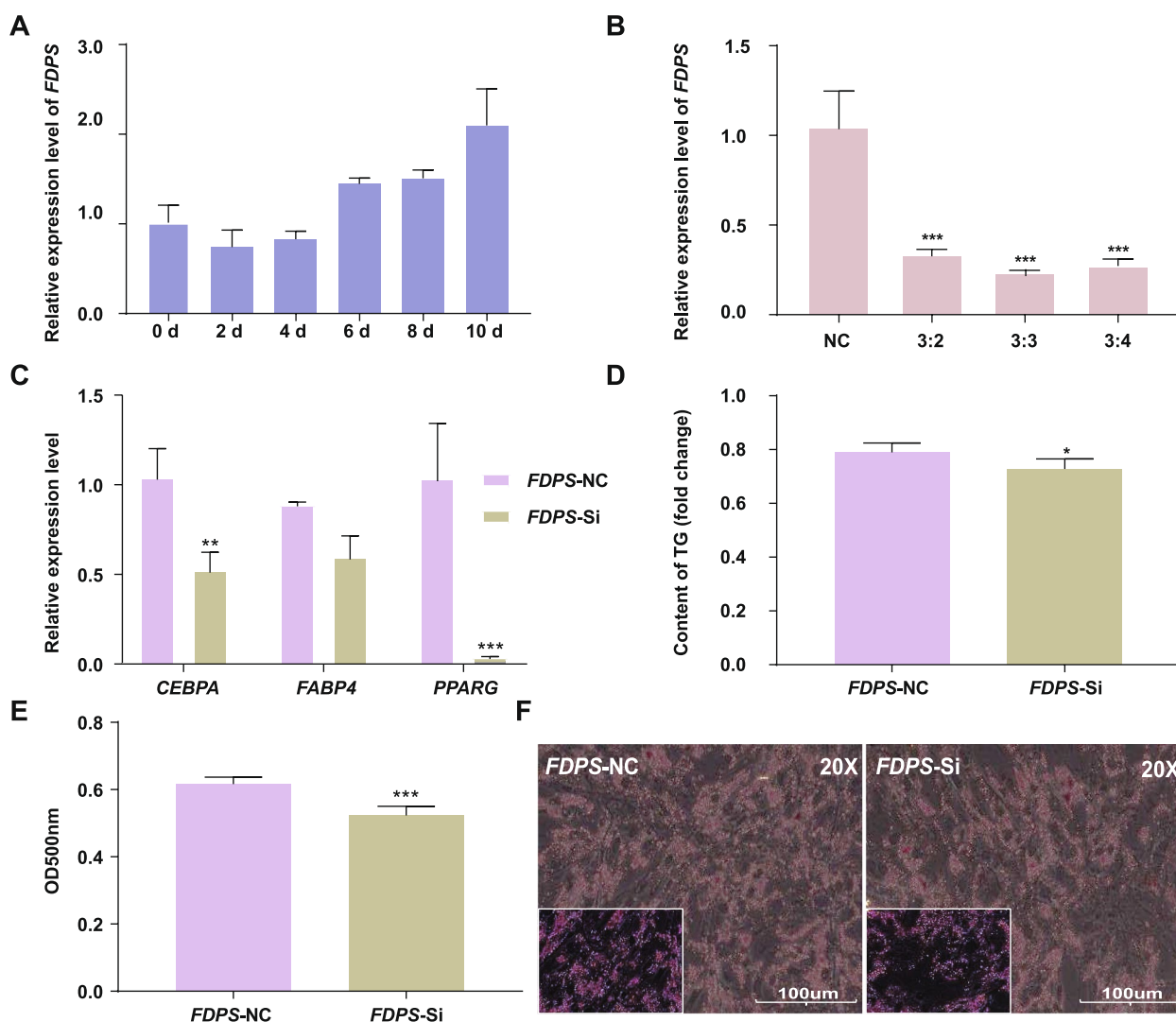


**Fig. 5** Interference with *FDPS* expression inhibits intramuscular preadipocyte differentiation. **A** mRNA levels of *FDPS* during the differentiation of chicken primary intramuscular adipocytes into mature adipocytes. **B** Relative expression of *FDPS* in intramuscular adipocytes transfected with *FDPS*. **C** Relative mRNA levels of adipocyte differentiation-related genes (*FABP4*, *FASN*, and *CEBPA*) after interference with *FDPS* expression. **D** The triglyceride content was determined by measurement of the absorbance at 500 nm after interference with *FDPS* expression. **E** Representative images of Oil Red O staining in intramuscular adipocytes transfected with *FDPS* siRNA or the corresponding NC (this image was acquired with a 20× objective, and an enlarged image is shown in the bottom left corner of the image). **F** Semiquantitative assessment of Oil Red O absorbance at 450 nm

adipocyte growth and development. Thus, we performed transcriptome sequencing of intramuscular adipocytes after transfection with the miR-128-3p mimic and inhibitor. In the comparison between the M group and SI group, 817 upregulated and 862 downregulated mRNAs were identified. Functional enrichment analysis revealed that the DEGs in the M group compared with the SI group were involved in the *PPAR* signaling pathway and *MAPK* signaling pathway, both of which are associated with fat deposition [36, 37]. Several DEGs were regarded as potentially regulating chicken preadipocyte

differentiation, for example, *APOA1* [38], *FDPS*, *MSMO1* [39], and *HMGCS1* [40]. More interestingly, miR-128-3p can target many genes that may be involved in lipid deposition, such as *FDPS*, *GGT5*, *TMEM37*, and *ASL2*, based on a comparison of their binding sites with the miR-128-3p seed region [41–45].

miRNAs bind to the 3'UTRs of mRNAs through their core seed region, and current research focuses on miRNAs that regulate lipid deposition through the lipogenic *PPAR-α* pathway [46], adiponectin receptor pathway, and *AMPK* pathway [47]. Through target prediction



and homology analysis, we found that the *FDPS* 3'UTR can efficiently bind to the miR-128-3p seed region. Our results showed that miR-128-3p can target the *FDPS* gene for binding and that overexpression of miR-128-3p decreased *FDPS* gene expression. Subsequently, we found that downregulation of *FDPS* inhibited intramuscular adipocyte differentiation. RT-qPCR analysis showed that after interference with *FDPS* expression, the expression of the adipose differentiation marker genes (*CEBPA* and *PPARG*) was significantly reduced, but there was no significant change in the expression level of *FABP4*. *PPARG* and *CEBPA* play important roles in early adipocyte differentiation, and recent studies have revealed that the *PPARG* and *CEBPA* target genes are colocalized [48]. Therefore, we speculate that there is a clear association among the expression of the *FDPS*, *PPAR*, and *CEBPA* genes, but the associations of these genes with *FABP4* are relatively weak. Studies have shown that genes related to cholesterol biosynthesis, carbohydrate metabolism and fatty acid biosynthesis impact fat development [49]. The mevalonate pathway is a metabolic pathway for the synthesis of isoprenyl pyrophosphate and dimethylallyl pyrophosphate from acetyl-CoA and is the major pathway of de novo cholesterol synthesis in cells [50]. *FDPS* is a branch point enzyme involved in the synthesis of sterols and prenylated cellular metabolites [51, 52]. Therefore, we hypothesized that *FDPS* may affect fat deposition by regulating cholesterol synthesis and affecting acetyl-CoA content. Together, our results indicate that *FDPS* is a functional target of miR-128-3p and can participate in adipogenesis, which is thus regulated by miR-128-3p.

## Conclusion

In conclusion, this study demonstrates that miR-128-3p can inhibit chicken intramuscular adipocyte differentiation by downregulating *FDPS*. Our findings provide a valuable resource for understanding IMF deposition and for explaining the genetic basis of traits related to meat quality in poultry.

## Materials and methods

### Primary intramuscular precursor adipocytes isolation and culture and induced differentiation

The intramuscular adipocytes were from the pectoral muscle tissue of 14-day-old Gushi chicken under sterile conditions [53]. Pectoral muscle tissue was separated using a scalpel and then was digested with collagenase type I (solaibao, Beijing, China) at 37 °C for 60 min. Briefly, the digested cell fraction was filtered sequentially passed through cell strainers (Biologix, Jinan, China) with pore sizes of 70 µm and 45 µm. The cell precipitate was centrifugated at 1000 rpm for 10 min. Subsequently, these cells were maintained in DMEM/F12 medium

(BI, Massachusetts, USA), supplemented with 10% fetal bovine serum (BI, Massachusetts, USA), and 1% penicillin/streptomycin (Solarbio) in an incubator with a 5% CO<sub>2</sub> atmosphere at 37 °C. After 2 h, the medium was changed. Once upon the confluence of cells reaching 90%, according to the hormone "cocktail method" is used to induce differentiation [54], and the complete medium would be replaced with the differentiation inducing medium (0.5 mM 3-isobutyl-1-methylxanthine (IBMX), 1 µM dexamethasone (Sigma), and 10 g/l insulin (Sigma)).

### Cell transfection

The miRNA mimic/inhibitor and siRNA interference sequences and their corresponding negative controls were purchased from Genechem (Shanghai, China). Cells were transfected with miRNA mimics, inhibitors and *FDPS*-SI with Liposome 2000 reagent (Invitrogen, USA) according to the manufacturer's instructions. Transfection was carried out when the cell confluence was 60–70%, and the medium was changed to complete medium after 6 h.

### CCK-8, EdU and cell cycle assay detection of cell proliferation

The intramuscular adipocytes proliferation was detected after 12 h, 24 h, 36 h and 48 h of transfection using a Trans Detect CCK-8 kit (Toyohito, Japan) according to the manufacturer's protocol. 10 µL of CCK-8 solution was added to the cells and incubated at 37 °C constant temperature incubator for 2 h. Then, the absorbance value was measured at 450 nm using the microplate reader.

The intramuscular adipocytes was detected using a Cell-Light EdU Apollo567 In Vitro Kit (RiboBio, Guangzhou, China) according to the manufacturer's protocol after transfection for 24 h. Briefly, 100 µL of 50 mm EdU reagent was added to each well and incubated for 2 h at 37 °C. After the staining, the camera was photographed in the dark under the fluorescent microscope. Finally, the Image J software was used to count the number of new cells.

The intramuscular adipocytes were seeded in 6 well cell culture plates. The cells were transfected with miR-128-3p mimic, miR-128-3p inhibitor, and negative control. After 48 h, Cells were collected, washed with cold PBS, and fixed with 70% ethanol at 20 °C for 6 h. Then the cells were washed with PBS and added for a final mass concentration of 50 mg/mL to incubate for 30 min at 37 °C. Subsequently, 400 µL of 50 µg/mL propidium iodide (PI) solution was added, and the cells were stained in the dark for 30 min at 25 °C. Finally, the cell cycle was observed by flow cytometry (FACS Calibur, BD Biosciences).



### Oil-Red O staining and triglyceride assay detection of cell differentiation

The intramuscular adipocytes samples were washed three times with PBS (Gibco, Carlsbad, CA, USA) and fixed with 4% paraformaldehyde for 30 min [55]. Subsequently, cells were stained with Oil-Red O working solution (Sigma) for 20 min after being washed with PBS. Then the intramuscular adipocytes were photographed by microscope. Lipid droplets were dissolved by Isopropyl alcohol and the absorbance value was calculated at 490 nm using microplate reader.

The intramuscular adipocytes samples were treated with 0.25% trypsin until separation and centrifuged for 3 min at 1000 rpm. After all, TG content in cell homogenate was determined using a triglyceride content detection kit (APPLYGEN, Beijing, China) according to the manufacturer's instructions. The protein concentrations were measured with the BCA Protein Assay Kit (EpiZyme, Shanghai, China) to normalize the TG content. The absorbance value was calculated at 550 nm using microplate reader.

### Collection of sequencing samples

The transfected miR-128-3p-mimics, miR-128-3p-inhibitor and miR-128-3p-NC were divided into over-expression group (M group), interference group (SI group), and blank treatment group (NC group), respectively. The total RNA was extracted using Trizol reagent (Vazyme, Nanjing, China). The expression of miR-128-3p was detected by fluorescent quantitative PCR. The sample with the highest overexpression efficiency ( $n=3$ ) and interference efficiency ( $n=3$ ) was collected, respectively, and sent to Nanjing Parsono Gene Technology Co., Ltd. for transcriptome sequencing.

### Transcriptome data analysis

After the removal of raw reads containing no insertion sequence, over 0.2% of poly-N, and low-quality paired reads, we obtained clean reads. The high-quality data (clean data) were mapped to the reference genome (GRCg7a) using TopHat2's upgraded HISAT2 software [56]. Read count values were aligned to each gene using HTSeq statistics as the gene's original expression quantity [57]. Differential gene expression analysis was conducted using DESeq [58], and differentially expressed genes (DEGs) were defined based on the following criteria:  $|\log_2 \text{fold change}| > 1$  and the  $P$  value  $< 0.05$ . The DEGs were subjected to functional annotation and pathway enrichment analysis using the KOBAS server [59].

### RT-qPCR

Total RNA was extracted from tissues and harvested cells using Trizol (Vazyme, Nanjing, China). Reverse

transcription of mRNA was performed using a HiScript II Q Select RT SuperMix for qPCR kit (Vazyme, Nanjing, China) according to manufacturer instructions. First step reaction system: 4  $\mu$ l, 4 $\times$ gDNA wiper Mix, Total RNA 1000 ng, added RNase free ddH<sub>2</sub>O to a total system of 16  $\mu$ l. The reaction procedure was set to 42 °C for 2 min and stored at 4 °C. Second step reaction system: 4  $\mu$ l, 5 $\times$ HiScript III qRT SuperMix was added to the previous product, resulting in a total system of 20  $\mu$ l. The reaction procedure was set as 37 °C for 15 min and 8 °C for 5 s. Finally, the product cDNA was diluted twice for subsequent fluorescence quantitative testing. We designed the PCR primers using Primer Premier 5, and the primer sequences were shown in Supplementary table 1. The ChamQ Universal SYBR qPCR Master Mix kit (Vazyme, Nanjing, China) was used to conduct quantitative real-time PCR (Q-qPCR). The total reaction volume was 10  $\mu$ l, and consisted of 1  $\mu$ l cDNA, 0.5  $\mu$ l reverse and forward primers (per gene), 5  $\mu$ l SYBR, and 3  $\mu$ l double-distilled water. The reaction procedure was performed under the following conditions: 95 °C for 30 s, followed by 40 cycles at 95 °C for 15 s, and 60 °C for 34 s. Finally, the melting curve is collected at 60–95 °C. Relative expression level was quantified by the  $2^{-\Delta\Delta C_t}$  [60] approach.  $\beta$ -actin and U6 was using as the normalization references for mRNA and miRNA, respectively.

### Dual luciferase reporter assay

The laboratory psiCHECK2 vector was used to construct the psiCHECK2-FDPS-3'UTR-WT and psiCHECK2-FDPS-3'UTR-MuT plasmids. They were transfected with miRNA-128-3p-mimics and psiCHECK2 vector into DF1 cells. After 48 h, the samples were collected, and the fluorescence activity was detected using the Dual-Glo Luciferase Assay System (Promega, Madison, WI, USA).

### Statistical analysis

Data analysis was performed with SPSS 26.0. All data was presented as "mean  $\pm$  standard error (SEM)". Significant differences between groups were analyzed using one-way ANOVA. Asterisks signify different significance levels (\* $P < 0.05$ , \*\* $P < 0.01$ , and \*\*\* $P < 0.001$ ).

### Abbreviations

IMF	Intramuscular fat
miRNA	MicroRNA
mRNA	Messenger RNA
NC group	Blank treatment group
M group	Mimics-treated group
SI group	Inhibitor-treated group
GO	Gene ontology
KEGG	Kyoto encyclopedia of genes and genomes

RT-qPCR	Quantitative real-time PCR
PBS	Phosphate buffered saline
CCK8	Cell Counting Kit-8
IRS2	Insulin receptor substrate 2
IRS1	Insulin receptor substrate 1
Akt	Serine-threonine kinase
LPIN1	Lipin 1
PPAR $\gamma$	Peroxisome proliferator-activated receptor $\gamma$
BMSC	Bone mesenchymal stem cell
FOXO1	Forkhead box protein O1
FOXO4	Forkhead box protein O4
SREBP	Sterol regulatory element-binding protein
ChREBP	Carbohydrate response element binding protein
FABP4	Fatty acid binding protein 4
FASN	Fatty acid synthetase
CEBPA	CCAAT/enhancer-binding protein alpha
BCL2	B-cell lymphoma-2
PCNA	Proliferating Cell Nuclear Antigen
APOA1	Apolipoprotein A1
FDPS	Farnesyl Diphosphate Synthase
MSMO1	Methylsterol Monooxygenase 1
HMGCS1	3-Hydroxy-3-Methylglutaryl-CoA Synthase 1
GGT5	Gamma-glutamyl transferase 5
TMEM37	Transmembrane protein 37
ASL2	Colletotrichum siamense Argininosuccinate lyase
ACOT13	Acyl-CoA thioesterase 13
GPAM	Glycerol-3-phosphate acyltransferase
HCC	Hepatocellular carcinoma
PIK3R1	Phosphoinositide-3-kinase regulatory subunit 1
MMP9	Matrix metalloproteinase 9

## Supplementary Information

The online version contains supplementary material available at <https://doi.org/10.1186/s12864-023-09649-y>.

**Additional file 1: Table S1.** q-PCR primer sequences. **Table S2.** Statistics of downstream data. **Table S3.** Data filtering analysis. **Table S4.** Sequencing data positioning. **Table S5.** RNA-Seq Map Statistics. **Table S6.** Partial lipid metabolism related genes. **Table S7.** Sl vs. M share gene Target gene.

**Additional file 2: Fig. S1.** Detection of miR-128-3p overexpression interference efficiency Q-PCR primer sequences. **Fig. S2.** Flow cytometry detection. Cell cycle analysis via flow cytometry after overexpression or interference of miR-128-3p. **Fig. S3.** Apoptosis detection. Cell apoptosis assay via flow cytometry after overexpression and interference of miR-128-3p. **Fig. S4.** GO-KEGG enrichment analysis.

## Acknowledgements

Not applicable.

## Authors' contributions

ShuaiPeng Zhu and Binbin Zhang conceived the project and designed the experiments. Tingqi Zhu, Dongxue Wang, Cong Liu, Yixuan Liu, Yuehua He and Wenjie Liang performed the animal experiments and sample collection. Wenting Li, Ruili Han, Donghua Li, Fengbin Yan provided valuable suggestion and comments to improve the manuscript with contributions from all other authors. Yadong Tian, Guoxi Li, Xiangtao Kang, Zhuanjian Li, Ruirui Jiang and Guirong Sun discussed the results. All authors have read and approved the manuscript.

## Funding

This work was supported by grants from the National Natural Science Foundation of China (32072710), the Scientific Studio of Zhongyuan Scholars (30601985) and the Key Research Project of the Shennong Laboratory (SN01-2022-05).

## Availability of data and materials

The RNA sequencing data used and analyzed during the current study are available from the NCBI (accession number: PRJNA986221).

## Declarations

### Ethics approval and consent to participate

All animal experiments were performed according to the Regulations for the Administration of Affairs Concerning Experimental Animals (Ministry of Science and Technology, China, 2004). The protocols and guidelines were approved by the Institutional Animal Care and Use Committee of Henan Agricultural University, China. All sections of this study adhere to the ARRIVE Guidelines for reporting animal research.

### Consent for publication

Not applicable.

### Competing interests

The authors declare no competing interests.

Received: 2 July 2023 Accepted: 4 September 2023

Published online: 12 September 2023

## References

- Jia J, Zhang H, Qu J, Wang Y, Xu N. Immunosensor of Nitrofurantol Antibiotics and Their Metabolites in Animal-Derived Foods. A Review *Frontiers in chemistry*. 2022;10:813666.
- Al-Khalaifah H, Al-Nasser A, Givens DL, Rymer C, Yaqoob P. Comparison of different dietary sources of n-3 polyunsaturated fatty acids on immune response in broiler chickens. *Heliyon*. 2020;6(1):e03326.
- Liu L, Liu X, Cui H, Liu R, Zhao G, Wen J. Transcriptional insights into key genes and pathways controlling muscle lipid metabolism in broiler chickens. *BMC Genomics*. 2019;20(1):863.
- Palma-Granados P, García-Casco JM, Caraballo C, Vázquez-Ortego P, Gómez-Carballar F, Sánchez-Esquiliche F, Óvilo C, Muñoz M. Design of a low-density SNP panel for intramuscular fat content and fatty acid composition of backfat in free-range Iberian pigs. *J Animal Sci*. 2023;101:1–8.
- Tian W, Wang Z, Wang D, Zhi Y, Dong J, Jiang R, Han R, Li Z, Kang X, Li H, et al. Chromatin Interaction Responds to Breast Muscle Development and Intramuscular Fat Deposition Between Chinese Indigenous Chicken and Fast-Growing Broiler. *Frontiers in cell and developmental biology*. 2021;9:782268.
- Yan W, Kan X, Wang Y, Zhang Y. Expression of key genes involved in lipid deposition in intramuscular adipocytes of sheep under high glucose conditions. *J Anim Physiol Anim Nutr*. 2023;107(2):444–52.
- Raza SHA, Khan R, Cheng G, Long F, Bing S, Easa AA, Schreurs NM, Pant SD, Zhang W, Li A, et al. RNA-Seq reveals the potential molecular mechanisms of bovine KLF6 gene in the regulation of adipogenesis. *Int J Biol Macromol*. 2022;195:198–206.
- Huang J, Feng X, Zhu R, Guo D, Wei Y, Cao X, Ma Y, Shi D. Comparative transcriptome analysis reveals that PCK1 is a potential gene affecting IMF deposition in buffalo. *BMC Genomics*. 2020;21(1):710.
- Xiao C, Wei T, Liu LX, Liu JQ, Wang CX, Yuan ZY, Ma HH, Jin HG, Zhang LC, Cao Y. Whole-Transcriptome Analysis of Preadipocyte and Adipocyte and Construction of Regulatory Networks to Investigate Lipid Metabolism in Sheep. *Front Genet*. 2021;12:662143.
- Zhang M, Lin W, Wu Q, Li Y, Chen D, Liu L, Sun Y. Effects of Dietary Vitamin E on Intramuscular Fat Deposition and Transcriptome Profile of the Pectoral Muscle of Broilers. *J Poult Sci*. 2023;60(1):2023006.
- Keren J, Meng Z, Donghua Li, Ruirui J, Ruili H, Yadong T, Xiangtao K, Guirong S. Comparative Analysis of Meat Quality Characteristics of Gushi Chickens at Different Weeks of Age. *Chinese Poultry*. 2017;39(001):15–9.
- Ma C, Qi X, Wei YF, Li Z, Zhang HL, Li H, Yu FL, Pu YN, Huang YC, Ren YX. Amelioration of ligamentum flavum hypertrophy using umbilical cord mesenchymal stromal cell-derived extracellular vesicles. *Bioactive Mater*. 2023;19:139–54.
- Zhao F, Wu L, Wang Q, Zhao X, Chen T, Yin C, Yan L, Yang X. Insulin-like growth factor 2 mRNA-binding protein 2-regulated alternative splicing of nuclear factor 1 C-type causes excessive granulosa cell proliferation in polycystic ovary syndrome. *Cell Prolif*. 2022;55(4):e13216.

14. Li J, Chen K, Dong X, Xu Y, Sun Q, Wang H, Chen Z, Liu C, Liu R, Yang Z, et al. YTHDF1 promotes mRNA degradation via YTHDF1-AGO2 interaction and phase separation. *Cell Prolif*. 2022;55(1):e13157.
15. Chen Y, Zhao Y, Jin W, Li Y, Zhang Y, Ma X, Sun G, Han R, Tian Y, Li H, et al. MicroRNAs and their regulatory networks in Chinese Gushi chicken abdominal adipose tissue during postnatal late development. *BMC Genomics*. 2019;20(1):778.
16. Subramaniam S, Jeet V, Clements JA, Gunter JH, Batra J. Emergence of MicroRNAs as Key Players in Cancer Cell Metabolism. *Clin Chem*. 2019;65(9):1090–101.
17. Jing Y, Cheng B, Wang H, Bai X, Zhang Q, Wang N, Li H, Wang S. The landscape of the long non-coding RNAs and circular RNAs of the abdominal fat tissues in the chicken lines divergently selected for fatness. *BMC Genomics*. 2022;23(1):790.
18. Zhang W, Raza SHA, Li B, Sun B, Wang S, Pant SD, Al-Abbas NS, Shaer NA, Zan L. miR-33a Inhibits the Differentiation of Bovine Preadipocytes through the IRS2-Akt Pathway. *Genes*. 2023;14(2):529.
19. Chao X, Guo L, Wang Q, Huang W, Liu M, Luan K, Jiang J, Lin S, Nie Q, Luo W, et al. miR-429-3p/LPIN1 Axis Promotes Chicken Abdominal Fat Deposition via PPAR $\gamma$  Pathway. *Front Cell Dev Biol*. 2020;8:595637.
20. Lin Z, He H, Wang M, Liang J. MicroRNA-130a controls bone marrow mesenchymal stem cell differentiation towards the osteoblastic and adipogenic fate. *Cell Prolif*. 2019;52(6):e12688.
21. Du G, Cheng X, Zhang Z, Han L, Wu K, Li Y, Lin X. TGF-Beta Induced Key Genes of Osteogenic and Adipogenic Differentiation in Human Mesenchymal Stem Cells and miRNA-mRNA Regulatory Networks. *Front Genet*. 2021;12:759596.
22. Chen C, Deng Y, Hu X, Ren H, Zhu J, Fu S, Xie J, Peng Y. miR-128-3p regulates 3T3-L1 adipogenesis and lipolysis by targeting Pparg and Sertad2. *J Physiol Biochem*. 2018;74(3):381–93.
23. Zhang M, Li F, Sun JW, Li DH, Li WT, Jiang RR, Li ZJ, Liu XJ, Han RL, Li GX, et al. LncRNA IMFNCR Promotes Intramuscular Adipocyte Differentiation by Sponging miR-128-3p and miR-27b-3p. *Front Genet*. 2019;10:42.
24. Sud N, Zhang H, Pan K, Cheng X, Cui J, Su Q. Aberrant expression of microRNA induced by high-fructose diet: implications in the pathogenesis of hyperlipidemia and hepatic insulin resistance. *J Nutr Biochem*. 2017;43:125–31.
25. Sun G, Li F, Ma X, Sun J, Jiang R, Tian Y, Han R, Li G, Wang Y, Li Z et al. gga-miRNA-18b-3p inhibits intramuscular adipocytes differentiation in chicken by targeting the ACOT13 gene. *Cells*. 2019;8(6):556.
26. Lin Z, Tang Y, Li Z, Li J, Yu C, Yang C, Liu L, Wang Y, Liu Y. miR-24-3p Dominates the proliferation and differentiation of chicken intramuscular preadipocytes by blocking ANXA6 Expression. *Genes*. 2022;13(4):635.
27. Dejure FR, Royle N, Herold S, Kalb J, Walz S, Ade CP, Mastrobuoni G, Vanselow JT, Schlosser A, Wolf E, et al. The MYC mRNA 3'-UTR couples RNA polymerase II function to glutamine and ribonucleotide levels. *EMBO J*. 2017;36(13):1854–68.
28. Wei Q, Li J, He H, Cao Y, Li D, Ameer FK, Zhang Y, Wang J, Yu C, Yang C, et al. miR-23b-3p inhibits chicken granulosa cell proliferation and steroid hormone synthesis via targeting GDF9. *Theriogenology*. 2022;177:84–93.
29. Zhang M, Han Y, Zhai Y, Ma X, An X, Zhang S, Li Z. Integrative analysis of circRNAs, miRNAs, and mRNAs profiles to reveal ceRNAs networks in chicken intramuscular and abdominal adipogenesis. *BMC Genomics*. 2020;21(1):594.
30. Li F, Li D, Zhang M, Sun J, Li W, Jiang R, Han R, Wang Y, Tian Y, Kang X, et al. miRNA-223 targets the GPAM gene and regulates the differentiation of intramuscular adipocytes. *Gene*. 2019;685:106–13.
31. Qu C, Liu X, Guo Y, Fo Y, Chen X, Zhou J, Yang B. MiR-128-3p inhibits vascular smooth muscle cell proliferation and migration by repressing FOXO4/MMP9 signaling pathway. *Mol Med (Cambridge, Mass)*. 2020;26(1):116.
32. Huang CY, Huang XP, Zhu JY, Chen ZG, Li XJ, Zhang XH, Huang S, He JB, Lian F, Zhao YN, et al. miR-128-3p suppresses hepatocellular carcinoma proliferation by regulating PIK3R1 and is correlated with the prognosis of HCC patients. *Oncol Rep*. 2015;33(6):2889–98.
33. Shi Y, Yan F, Wang F, Pan L. MiR-128-3p suppresses tumor proliferation and metastasis via targeting CDC6 in hepatocellular carcinoma cells. *Tissue Cell*. 2021;72:101534.
34. Shen X, Liu Z, Cao X, He H, Han S, Chen Y, Cui C, Zhao J, Li D, Wang Y, et al. Circular RNA profiling identified an abundant circular RNA circTMTTC1 that inhibits chicken skeletal muscle satellite cell differentiation by sponging miR-128-3p. *Int J Biol Sci*. 2019;15(10):2265–81.
35. Shi L, Zhou B, Li P, Schinckel AP, Liang T, Wang H, Li H, Fu L, Chu Q, Huang R. MicroRNA-128 targets myostatin at coding domain sequence to regulate myoblasts in skeletal muscle development. *Cell Signal*. 2015;27(9):1895–904.
36. Ma X, Yang X, Zhang D, Zhang W, Wang X, Xie K, He J, Mei C, Zan L. RNA-seq analysis reveals the critical role of the novel lncRNA BIANCR in intramuscular adipogenesis through the ERK1/2 signaling pathway. *J Animal Sci Biotechnol*. 2023;14(1):21.
37. Kong Y, Liu C, Zhang X, Liu X, Li W, Li F, Wang X, Yue X. Characterization of fatty acid compositions in longissimus thoracis muscle and identification of candidate gene and SNPs related to polyunsaturated fatty acid in Hu sheep. *J Animal Sci*. 2023;101:1–15.
38. Kastrenopoulou A, Kypreos KE, Papachristou NI, Georgopoulos S, Mastora I, Papadimitriou-Olivgeri I, Spentzopoulou A, Nikitovic D, Kontogeorgakos V, Blair HC, et al. ApoA1 Deficiency Reshapes the Phenotypic and Molecular Characteristics of Bone Marrow Adipocytes in Mice. *Int J Mol Sci*. 2022;23(9):4834.
39. Xin Y, Li C, Guo Y, Xiao R, Zhang H, Zhou G. RNA-Seq analysis reveals a negative role of MSMO1 with a synergized NSDHL expression during adipogenesis of 3T3-L1. *Biosci Biotechnol Biochem*. 2019;83(4):641–52.
40. Reijnders D, Olson KN, Liu CC, Beckers KF, Ghosh S, Redman LM, Sones JL. Dyslipidemia and the role of adipose tissue in early pregnancy in the BPH/5 mouse model for preeclampsia. *Am J Physiol Regul Integr Comp Physiol*. 2019;317(1):R49–r58.
41. Wang X, Zhang X, Chen Y, Zhao C, Zhou W, Chen W, Zhang C, Ding K, Li W, Xu H, et al. Cardiac-specific deletion of FDPS induces cardiac remodeling and dysfunction by enhancing the activity of small GTP-binding proteins. *J Pathol*. 2021;255(4):438–50.
42. Solimena M, Schulte AM, Marselli L, Ehehalt F, Richter D, Kleeberg M, Mzi- aut H, Knoch KP, Parnis J, Bugliani M, et al. Systems biology of the IMIDIA biobank from organ donors and pancreatectomised patients defines a novel transcriptomic signature of islets from individuals with type 2 diabetes. *Diabetologia*. 2018;61(3):641–57.
43. Liu C, Tao Y, Lin H, Lou X, Wu S, Chen L. Classification of stomach adenocarcinoma based on fatty acid metabolism-related genes profiling. *Front Mol Biosci*. 2022;9:962435.
44. Wen F, Huang J, Lu X, Huang W, Wang Y, Bai Y, Ruan S, Gu S, Chen X, Shu P. Identification and prognostic value of metabolism-related genes in gastric cancer. *Aging*. 2020;12(17):17647–61.
45. Nagasaki A, Gotoh T, Takeya M, Yu Y, Takiguchi M, Matsuzaki H, Takatsuki K, Mori M. Coinduction of nitric oxide synthase, argininosuccinate synthetase, and argininosuccinate lyase in lipopolysaccharide-treated rats. RNA blot, immunoblot, and immunohistochemical analyses. *J Biol Chem*. 1996;271(5):2658–62.
46. Laezza C, D'Alessandro A, Di Croce L, Picardi P, Ciaglia E, Pisanti S, Malfitano AM, Comegna M, Faraonio R, Gazzero P, et al. p53 regulates the mevalonate pathway in human glioblastoma multiforme. *Cell Death Dis*. 2015;6(10):e1909.
47. Li B, Huang X, Yang C, Ge T, Zhao L, Zhang X, Tian L, Zhang E. miR-27a Regulates Sheep Adipocyte Differentiation by Targeting CPT1B Gene. *Animals*. 2021;12(1):28.
48. Rosen ED. The molecular control of adipogenesis, with special reference to lymphatic pathology. *Ann N Y Acad Sci*. 2002;979:143–58 (discussion 188–196).
49. Claire D'Andre H, Paul W, Shen X, Jia X, Zhang R, Sun L, Zhang X. Identification and characterization of genes that control fat deposition in chickens. *J Animal Sci Biotechnol*. 2013;4(1):43.
50. Rashkovan M, Albero R, Gianni F, Perez-Duran P, Miller HI, Mackey AL, Paietta EM, Tallman MS, Rowe JM, Litzow MR, et al. Intracellular Cholesterol Pools Regulate Oncogenic Signaling and Epigenetic Circuitries in Early T-cell Precursor Acute Lymphoblastic Leukemia. *Cancer Discov*. 2022;12(3):856–71.
51. Ayoub HM, McDonald MR, Sullivan JA, Tsao R, Meckling KA. Proteomic Profiles of Adipose and Liver Tissues from an Animal Model of Metabolic Syndrome Fed Purple Vegetables. *Nutrients*. 2018;10(4):456.
52. Ciaglia E, Pisanti S, Picardi P, Laezza C, Malfitano AM, D'Alessandro A, Gazzero P, Vitale M, Carbone E, Bifulco M. N6-isopentenyladenosine, an endogenous isoprenoid end product, directly affects cytotoxic and regulatory functions of human NK cells through FDPS modulation. *J Leukoc Biol*. 2013;94(6):1207–19.

53. Gan L, Yan J, Liu Z, Feng M, Sun C. Adiponectin prevents reduction of lipid-induced mitochondrial biogenesis via AMPK/ACC2 pathway in chicken adipocyte. *J Cell Biochem*. 2015;116(6):1090–100.
54. Tristan CA, Hong H, Jethmalani Y, Chen Y, Weber C, Chu PH, Ryu S, Jovanovic VM, Hur I, Voss TC, et al. Efficient and safe single-cell cloning of human pluripotent stem cells using the CEPT cocktail. *Nat Protoc*. 2023;18(1):58–80.
55. Zhang M, Li DH, Li F, Sun JW, Jiang RR, Li ZJ, Han RL, Li GX, Liu XJ, Kang XT, et al. Integrated Analysis of MiRNA and Genes Associated with Meat Quality Reveals that Gga-MiR-140-5p Affects Intramuscular Fat Deposition in Chickens. *Cell Physiol Biochem*. 2018;46(6):2421–33.
56. Gan Q, Luan M, Hu M, Liu Z, Zhang Z. Functional study of CYP90A1 and ALDH3F1 gene obtained by transcriptome sequencing analysis of *Brassica napus* seedlings treated with brassinolide. *Front Plant Sci*. 2022;13:1040511.
57. Dong J, Liu L, Chen L, Xiang Y, Wang Y, Zhao Y. The Coexistence of Bacterial Species Restructures Biofilm Architecture and Increases Tolerance to Antimicrobial Agents. *Microbiology spectrum*. 2023;11(2):e0358122.
58. Lamarre S, Frasse P, Zouine M, Labourdette D, Sainderichin E, Hu G, Le Berre-Anton V, Bouzayen M, Maza E. Optimization of an RNA-Seq Differential Gene Expression Analysis Depending on Biological Replicate Number and Library Size. *Front Plant Sci*. 2018;9:108.
59. Peng C, Li J, Ke X, Liu F, Huang KE. In silico and in vivo demonstration of the regulatory mechanism of Qi-Ge decoction in treating NAFLD. *Ann Med*. 2023;55(1):2200258.
60. Stocks MB, Moxon S, Mapleson D, Woolfenden HC, Mohorianu I, Folkes L, Schwach F, Dalmay T, Moulton V. The UEA sRNA workbench: a suite of tools for analysing and visualizing next generation sequencing microRNA and small RNA datasets. *Bioinformatics (Oxford, England)*. 2012;28(15):2059–61.

## Publisher's Note

Springer Nature remains neutral with regard to jurisdictional claims in published maps and institutional affiliations.

Ready to submit your research? Choose BMC and benefit from:

- fast, convenient online submission
- thorough peer review by experienced researchers in your field
- rapid publication on acceptance
- support for research data, including large and complex data types
- gold Open Access which fosters wider collaboration and increased citations
- maximum visibility for your research: over 100M website views per year

At BMC, research is always in progress.

Learn more [biomedcentral.com/submissions](https://biomedcentral.com/submissions)

